AGU PUBLICATIONS

JGR

Journal of Geophysical Research: Earth Surface

RESEARCH ARTICLE
10.1002/2015JF003522

Special Section:
Glacier Surging and Ice Streaming

Key Points:
- Horcones Inferior Glacier surged in 2002–2006 and the front advanced 3.1 km
- Velocities were derived from ASTER image cross correlation in COSI-Corr
- Horcones Inferior Glacier surge shows an Alaska-type hydrological switch

Supporting Information:
- Tables S1 and S2

Correspondence to:
P. Pitte,
pierrepitte@mendoza-conicet.gob.ar

Citation:
Pitte, P., E. Berthier, M. H. Masiokas, V. Cabot, L. Ruiz, L. Ferri Hidalgo, H. Gargantini, and L. Zalazar (2016), Geometric evolution of the Horcones Inferior Glacier (Mount Aconcagua, Central Andes) during the 2002–2006 surge, *J. Geophys. Res. Earth Surf.*, *121*, 111–127, doi:10.1002/2015JF003522.

Received 2 MAR 2015
Accepted 17 DEC 2015
Accepted article online 21 DEC 2015
Published online 21 JAN 2016

Geometric evolution of the Horcones Inferior Glacier (Mount Aconcagua, Central Andes) during the 2002–2006 surge

Pierre Pitte[1], Etienne Berthier[2], Mariano H. Masiokas[1], Vincent Cabot[2,3], Lucas Ruiz[1], Lidia Ferri Hidalgo[1], Hernán Gargantini[1], and Laura Zalazar[1]

[1]Instituto Argentino de Nivología, Glaciología y Ciencias Ambientales (CONICET), Mendoza, Argentina, [2]Laboratoire d'Études en Géophysique et Océanographie Spatiales, Université de Toulouse, Toulouse, France, [3]Now at Delft University of Technology, Delft, Netherlands

Abstract The Central Andes of Chile and Argentina (31–35°S) contain a large number and variety of ice masses, but only two surging glaciers have been studied in this region. We analyzed the 2002–2006 surge of the Horcones Inferior Glacier, Mount Aconcagua, Argentina, based on medium spatial resolution (15–30 m) satellite images and digital elevation models. During the buildup phase the glacier was stagnant, with velocities lower than 0.1 m/d. In the active-phase velocities reached 14 m/d and the glacier front advanced 3.1 km. At the peak of the active phase (2003–2004), the area-averaged elevation change was −42 m in the reservoir zone (2.53 km^2) and +30 m in the receiving zone (3.31 km^2). The estimated ice flux through a cross section located at 4175 meter above sea level was 10^8 m^3 during a period of 391 days, a flux that suggests a mean glacier thickness at this location of ~90 m. The depletion phase showed a recovery of the reservoir zone elevation, the down wasting of the receiving zone (−17 m, 2007–2014), and a return to quiescent velocities. The short active phase, the abrupt change in the velocities, and the high level of the proglacial stream indicate a hydrological switch (Alaska type) trigger. The 2002–2006 and 1984–1990 surges of Horcones Inferior were synchronous with the surges of nearby Grande del Nevado Glacier. These events occurred after periods of positive mass balance, so we hypothesize a climate driver.

1. Introduction

A surging glacier oscillates between long periods (tens to hundreds of years) of slow flow and shorter periods of typically 10–1000 times faster flow [*Post*, 1969]. During a surge, a large volume of ice is transported down valley from the reservoir zone to the receiving zone, which can result in a marked frontal advance. Two mechanisms have been proposed to explain the switch between these flow modes. The Alaskan type (hydrological switch) is a change in the basal hydrology from a channelized to a distributed linked cavity system which produces an abrupt switch between quiescent and surge velocities (e.g., Variegated Glacier) [*Kamb*, 1987; *Eisen et al.*, 2001]. The Svalbard type (thermal switch) is a thermally induced instability of the bed sediments under polythermal glaciers that shows a long period (up to several years) of steady acceleration, followed by a short period of relatively rapid acceleration and finally a gradual slowdown [*Truffer et al.*, 2000; *Murray et al.*, 2003; *Jiskoot and Juhlin*, 2009].

In general, the surge cycle can be divided into three phases. The first phase is the "buildup" of the surge, when the ice flow is temporarily reduced, the glacier surface rises and the longitudinal elevation profile becomes steeper. In the "active" or "surge" phase velocities increase sharply, and a wave of fast flow propagates down the glacier. Finally, in the "depletion" phase, compaction and ablation flatten the glacier surface and most of the surge-related crevasses close [*Dolgoushin and Osipova*, 1975]. The return time of the surges is thought to be influenced, in part, by periods of positive mass balance [*Cuffey and Paterson*, 2010]. Most surge-type glaciers occur within a well-defined climatic envelope of −10°C to 0°C mean annual air temperature and 165 to 2250 mm mean annual precipitation, with larger glaciers more prone to surging [*Sevestre and Benn*, 2015]. One of the most striking facts about surge-type glaciers is their tendency to cluster within particular regions, for example, Western North America [*Post*, 1969], East Greenland [*Jiskoot et al.*, 2003], Iceland [*Björnsson et al.*, 2003], Svalbard [*Jiskoot et al.*, 1998], Pamir [*Kotlyakov et al.*, 2008], and Karakoram [*Copland et al.*, 2011].

Glacier surges in the Central Andes of Chile and Argentina (31–35°S) [*Lliboutry*, 1999] have been reported since the early twentieth century. The Horcones Inferior Glacier (HI), which originates below the south face

of Mount Aconcagua (6962 meter above sea level (m asl), 32.65°S, 70.01°W), has undergone two relatively well documented surges in recent decades. Between December 1984 and January 1990 a surge wave propagated 3.5 km downward from the reservoir zone [*Happoldt and Schrott*, 1993; *Unger et al*., 2000]. After 1990, the glacier entered a quiescent phase. In February 2004, climbers reported that abnormally high proglacial runoff washed away the footbridge which was installed over the Horcones Inferior River in 1999. The glacier front advanced at unusual high rates of 10–30 m, forcing in the relocation of Confluencia Camp to its current position on top of a flat sandy hill, away from the HI.

The Grande del Nevado Glacier in the Plomo massif (33.10°S, 70.06°W, 50 km south of HI) is another glacier known for its surge behavior. The first documented surge of this glacier triggered a glacier lake outburst flood on January 1934 which destroyed large swaths of the Mendoza River valley including bridges of the international road and railroad, a hotel, and a hydropower station many kilometers downstream from the glacier. The flood, estimated at 6.7×10^7 m^3 of water [*King*, 1934], originated by the damming of the Plomo River by a 4.5 km advance of the Grande del Nevado Glacier. The glacier underwent a second surge event between February and November of 1984 when the front advanced 2.7 km and dammed the Plomo River again. A lake was formed again upstream from the ice dam but drained gradually underneath the ice during 1985 [*Espizua and Bengochea*, 1990]. A third surging event was observed with an advance of the glacier front in 2006, which again formed an ice-dammed lake that drained gradually through a subglacial channel.

Several other glaciers in the Central Andes of Chile and Argentina are reported to have surged during the twentieth century, including Colina, río Museo, Juncal Sur [*Helbling*, 1935], Piuquenes [*Rothlisberger*, 1986], Nieves Negras [*Lliboutry*, 1956], del Rio, este del Cerro Polleras, este del Cerro Marmolejo, and noreste del Cerro Alto [*Lliboutry*, 1999]. Nevertheless, no detailed studies have been carried out at these sites: velocity, elevation changes, volume of displaced ice, and timing of the events are almost entirely unknown.

The objective of this paper is to describe and analyze the 2002–2006 HI surge with remotely sensed data. We examine the temporal evolution of the glacier surface velocity through cross correlation of optical satellite images. We also quantify the ice volume transferred through the analysis of multiple digital elevation models (DEM). We selected HI for its documented past surge activity, its location along the ascending route to Mount Aconcagua and for the availability of numerous satellite images and DEMs for the study of the 2002–2006 event. To place this event in a wider context, we compare it with the earlier surge of HI (1985–1989) and also with the two most recent surges of the Grande del Nevado Glacier, in the nearby Plomo massif. We also investigate the possible influence of a regional climatic forcing on these surging events. Finally, we discuss analogies with the Karakoram region, where numerous surge-type glaciers have been identified and studied.

1.1. Horcones Inferior Glacier Setting

HI is a regenerated, debris-covered valley glacier which is fed by avalanches coming down from the hanging glaciers of the south face of Mount Aconcagua (Figure 1a). In 2003, before its last surge, this glacier was 8.2 km long, had a maximum width of 0.7 km, and covered an area of 5.2 km^2. The upper reaches of the glacier are formed by avalanche cones that descend to 4450 m asl, while the snout in 2003 was at 3850 m asl. A 2.8 km long rock glacier coming from a tributary valley terminates near the front position of HI (Figure 1). The glacier tongue is extensively covered with supraglacial debris, 0.1–2 m thick, and numerous small supraglacial lakes or thermokarst which are common features in the Central Andes (Figures 1c and 1d). The glacier flows southeast to south, following a valley that has a series of well-preserved lateral and terminal moraines.

In the Central Andes, precipitation is largely concentrated during the cold season, May–September, and shows strong year-to-year variations [*Masiokas et al*., 2006]. Maximum snow water equivalent (w.e.) measured between 2000 and 2011, at 3000 m asl in the Horcones valley, varied between 50 and 650 mm w.e., but older records indicate values as high as 1000 mm w.e. during snowy years such as 1982. Mean annual temperature is 5.7°C and the elevation of the mean annual 0°C isotherm is around 3600 m asl [*Carrasco et al*., 2008]. In this region, glaciers have retreated throughout the twentieth century [*Masiokas et al*., 2009]. Las Vacas and Güssfeldt glaciers, in the Aconcagua massif, have shown a slight recovery in 1980s, followed by enhanced recession in 1990s and moderate loss in the past decade [*Espizua and Pitte*, 2009]. Available mass balance from the small nearby Piloto Glacier (32.59°S, 70.14°W) [*Leiva et al*., 2007] and Echaurren Norte Glacier in Chile (33.58°S, 70.13°W) [*Escobar et al*., 1995; *World Glacier Monitoring Service* (*WGMS*), 2013] shows a negative

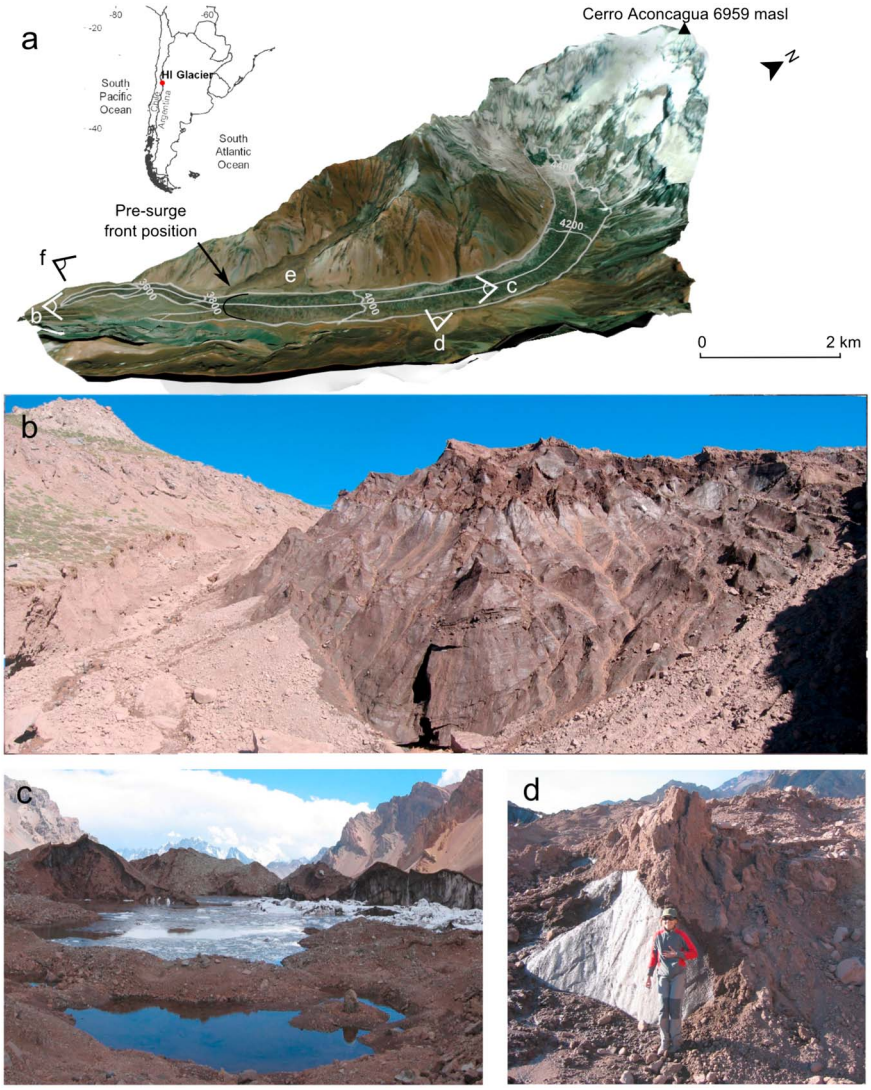

Figure 1. (a) Horcones Inferior Glacier (Quickbird image of 5 December 2005 draped on SRTM DEM). This is an oblique view so the scale is approximate. The locations and view directions of the field photos shown in this figure and in Figure 5 are indicated. (b) Glacier front (20 December 2007, photo L. Ferri Hidalgo). (c) Thermokarst on the glacier surface (19 December 2007, photo P. Pitte). (d) Thick debris cover of the glacier (17 December 2006, photo: H. Gargantini).

cumulative mass balance over the past 30 years, with some periods of minor recovery. Meltwater from the southern face of Mount Aconcagua drains through the Horcones Inferior River which, together with the Horcones Superior River, flows into Las Cuevas River, one of the three main tributaries of the Mendoza River. This river, with a mean discharge of less than 50 m^3/s, provides water to over 1 million people and 1500 km^2 of irrigated lands in the northern oasis of the Mendoza province [*Masiokas et al.*, 2006].

2. Data and Methods

2.1. Images and DEM

This work is based on 15–30 m spatial resolution, optical Advanced Spaceborne Thermal Emission and Reflection Radiometer (ASTER), Landsat TM, and Landsat ETM+ satellite images. Scenes from all seasons were considered, but wintertime, June–August, is largely underrepresented due to extensive cloud and snow cover. A total of 32 scenes were selected spanning from 13 January 2001 to 27 March 2010 (Figure 2a and Table S1 in the supporting information).

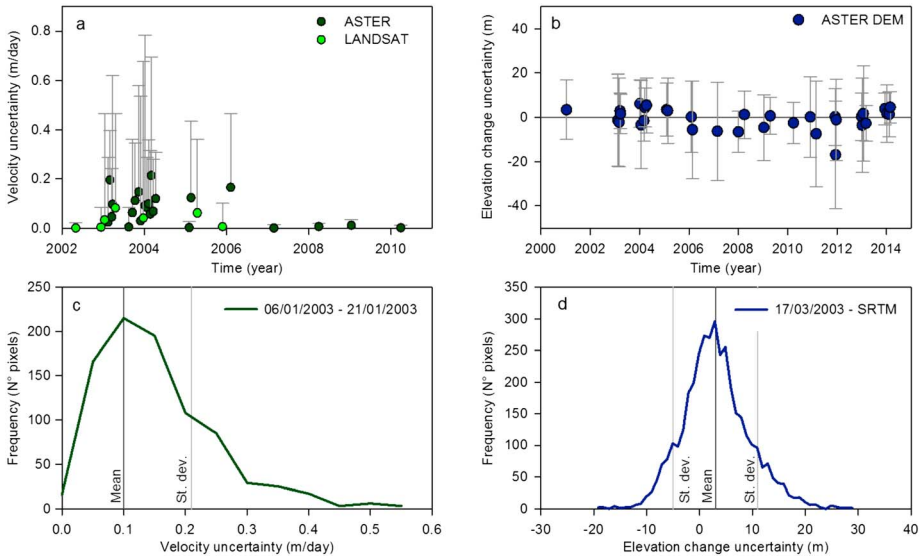

Figure 2. (a) ASTER and LANDSAT images acquisition dates and uncertainty in the resulting velocity fields estimated with the mean velocity (± standard deviation) of the displacements over stable control areas between every pair of successive images (listed in Table S1). (b) ASTER DEM dates and uncertainty in the elevation estimated with the mean elevation change residuals (± standard deviation) over the control areas between every ASTER DEM (listed in Table S2) and the SRTM DEM. Example of the distribution of the velocity uncertainty of an (c) image pair and a (d) DEM pair, indicated in the legend. The mean ($\pm\sigma$) is shown with vertical lines.

A total of 33 ASTER DEMs were processed (Figure 2b and Table S2). The ASTER DEMs are derived from 15 m spatial resolution, optical band 3: 0.78 to 0.86 μm stereo images, and have a 10 to 20 m vertical accuracy [*Hirano et al*., 2003; *Berthier et al*., 2010]. All available ASTER DEMs from the summer season, December–April, over the period 2001–2014 were considered. The Shuttle Radar Topography Mission DEM (SRTM) was also used. This DEM is derived from differential interferometry applied to radar C band images, has a grid cell size of 3 arc seconds, roughly 80 m × 90 m in the Mount Aconcagua region, and a reported vertical accuracy of ±6 m [*Farr et al*., 2007].

2.2. Satellite Image Processing

Glacier displacements were derived from the cross correlation of optical images through a two-step routine: the Coregistration of Optically Sensed Images and Correlation software package (COSI-Corr) [*Leprince et al*., 2007]. This is a free plug-in for the ENVI software. The first step produces a fine orthorectification of the raw satellite image. This procedure requires a base image (master: Landsat), a raw image with its ancillary data (slave: Level 1A ASTER scenes), and a DEM (e.g., SRTM). An initial set of tie points is manually selected on stable areas, converted to ground control points, and optimized by the software through cross correlation. All the raw slave images are then accurately orthorectified and coregistered with a subpixel accuracy. ASTER band 2 and LANDSAT TM band 3 which are on the 0.63–0.69 μm wavelength were used together with Band 8 from LANDSAT ETM+, which has a broader spectral length (0.52–0.9 μm) but a higher spatial resolution (15 m). LANDSAT TM scenes were oversampled to 15 m to match the resolution of the ASTER and LANDSAT ETM+ images.

The second step involves the correlation of the coregistered orthoimages and the calculation of the displacement fields (north-south and east-west) and the signal-to-noise ratio (SNR). The software allows a multiscale correlation which yielded optimum results with a 32 (initial) to 16 (final) pixel window size and a 4 pixel step. These parameters are a compromise between the image pixel size and the expected motion of the glacier. However, in some cases when the displacements were too large, the initial correlation window was extended from 32 to 64 pixels. The current version of COSI-Corr supports push broom sensors (ASTER) but not whisk broom sensors (LANDSAT TM and ETM+). Therefore, an orthorectified LANDSAT image was used as a base (master), and the following/previous ASTER scenes (slave) were adjusted to it. This procedure maintained the subpixel accuracy of the measurements but left a 1–8 m offset in the resulting displacement fields.

The total displacement and the displacement direction were calculated with the motion fields. Spurious, false positive values were removed using three sequential filters [*Berthier et al*., 2005; *Scherler et al*., 2008; *Herman et al*., 2011; *Quincey et al*., 2015]: First, a filter on the correlation score of the image pairs was applied to exclude poorly correlated pixels, i.e., SNR $>$ 0.975. Then a direction filter was used to exclude pixels showing anomalous flow directions, outside ±45° from the main flow line direction. A magnitude filter was applied to exclude pixels showing isolated very high motion values, greater than three standard deviations of the surrounding values. Finally, velocities were calculated taking into account the number of days between acquisitions (Table S1).

2.3. DEM Processing

In order to calculate elevation changes we subtracted the successive DEM pairs. The differencing was performed after 3-D coregistration of the ASTER DEMs to the reference SRTM DEM. First, we horizontally coregistered all DEMs through the minimization of the standard deviation of the elevation difference on the stable areas surrounding glaciers [*Berthier and Toutin*, 2008]. Then we corrected the vertical offsets between each ASTER DEM and the SRTM DEM on ice-free, stable, low slope and well-illuminated pixels. As a result, we obtained a set of 33 ASTER DEMs adjusted to the SRTM DEM.

In order to estimate the ice volume that was transferred from the reservoir to the receiving zone at the peak of the active phase, the volume change was calculated by subtracting the 11 April 2004 to the 17 March 2003 ASTER DEMs. In the resulting elevation change map we identified the reservoir zone which showed negative elevation difference values (mass loss), the receiving zone which showed positive elevation values (mass gain), and the boundary between both which had 0 m elevation change. We also made a rough estimate of the mean thickness of the glacier at this cross section of 0 m elevation change, considering the ice volume transferred, the mean velocity, and the section width.

2.4. Data Extraction

The outline and the central flow line of the glacier (Figure 1a) were hand digitized on the 2007 ASTER scene. Visual interpretation and hand digitizing are standard procedures for mapping debris-covered ice which cannot be accurately identified with automatic methods [*Paul et al*., 2013]. We consider the technique to be accurate within 1 pixel. The origin of the flow line is assumed to be the base of the south face of Mount Aconcagua, while the position of the snout for the last 20 years was 8.2 km away. Velocities and elevation changes were extracted along the central flow line. Elevation changes are reported in meters as mean values ± standard deviation along the center flow line in the reservoir or receiving zone.

2.5. Uncertainties Assessment

Uncertainties in the surface displacement measurements arise from errors in the coregistration, the quality of the images, and the performance of the correlation algorithm. All sources add up in the resulting displacement fields and can be estimated by taking measurements over stable terrain [*Berthier et al*., 2005; *Scherler et al*., 2008]. We calculated the velocity uncertainty by measuring the total displacement of areas of gently sloping ($<$25°), motionless terrain and then dividing these displacements by the number of days between acquisitions (Table S1). This showed that measured velocities have an average uncertainty of 0.1 ± 0.3 m/d (mean ± standard deviation, Figure 2a).

We treated each ASTER DEM similarly, selecting a sector of stable, gently sloping ($<$25°) terrain in the vicinity of HI and obtaining the elevation differences with the SRTM (Table S2). This showed that the DEMs are mostly unbiased with a mean elevation difference of −0.5 m ± 14 m (Figure 2b).

3. Results

3.1. Buildup Phase

The velocities between 2001 and 2010, measured along the flow line are shown in Figure 3. During the buildup phase (13 January 2001 to 11 December 2002) velocities were consistently low (below 0.1 m/d, Figure 3a). In the upper reaches of the glacier only isolated measurements were obtained, and no coherent spatial pattern was observed. Partial cloud and snow cover precluded the correlation of the images. During this time 80% of the values were removed by the directional filter, indicating the measurements are within

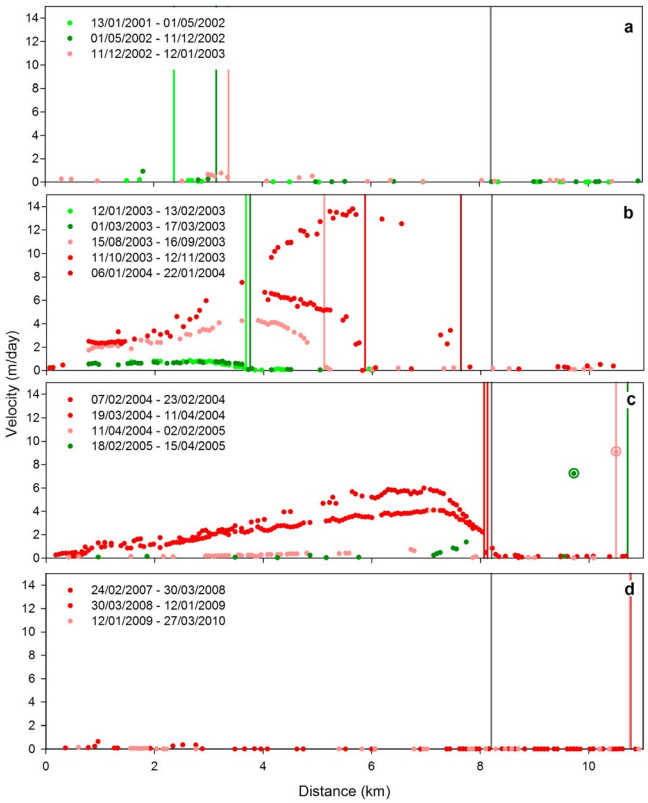

Figure 3. Velocity profiles during the buildup (a), active (b-c) and depletion (d) phases of the HI surge. The active phase was separated in two (b-c) to depict the acceleration and slowdown. Velocities are derived from a pair of optical images indicated in the legend and are represented in a green to red scale for increasing values. Vertical lines show the position of the surge wave and the pre-surge position of the front (gray). The circled values in Figure 3c are individual measurements of the glacier front advance, after 11 April 2004, when the correlation between images is lost (see text).

the error of the method. From 11 December 2002 to 12 January 2003 a slight pattern of motion can be detected (0.7 m/d) 3 km from the south face of Mount Aconcagua.

The elevation changes along the flow line relative to February 2000 are shown in Figure 4. In the buildup phase between February 2000 and January 2003, the average elevation change in the reservoir zone was 8 ± 7 m, but the data are limited. The quality of the 13 January 2001 ASTER DEM is poor, and no other topographic information is available for that period. The elevation data are worse in the upper 3.6 km, where snow cover is common, and also in the area immediately in front of the glacier snout (after 8.2 km). The latter is probably due to the fact that the flow line is located in a narrow valley (250 m wide) with steep walls (30 m), where the shading is strong.

3.2. Active Phase

The strongest acceleration of the glacier occurred between 12 January 2003 and 22 January 2004, when a wave of ice propagated 4 km downward at velocities that increased from 0.7 to 14 m/d (Figure 3b). This high-velocity pattern continued during the winter of 2003 despite the seasonal cooling. The end of winter (August–September 2003) showed intermediate velocities (4 m/d) between the 2002–2003 summer (0.6 m/d) and the 2003–2004 summer (10 m/d). Following this period, velocities decreased markedly to 6 m/d until 11 April 2004 (Figure 3c). After 11 April 2004, the surge wave overrode the former glacier front position and started a rapid descent through the Horcones Inferior river valley. The correlation algorithm failed to track features in this area due to extensive deformation of the glacier surface while advancing through the narrow (250 m) lower valley channel. Only one isolated value of 7.2 m/d could be obtained on the February 2005 to April 2005 profile. This value, identified by the magnitude filter as a potential outlier, was nonetheless included in Figure 3c (circled) because visual examination of the image pair suggested that it is probably a valid indicator of ice velocity at this point. The interpretation of the satellite images showed

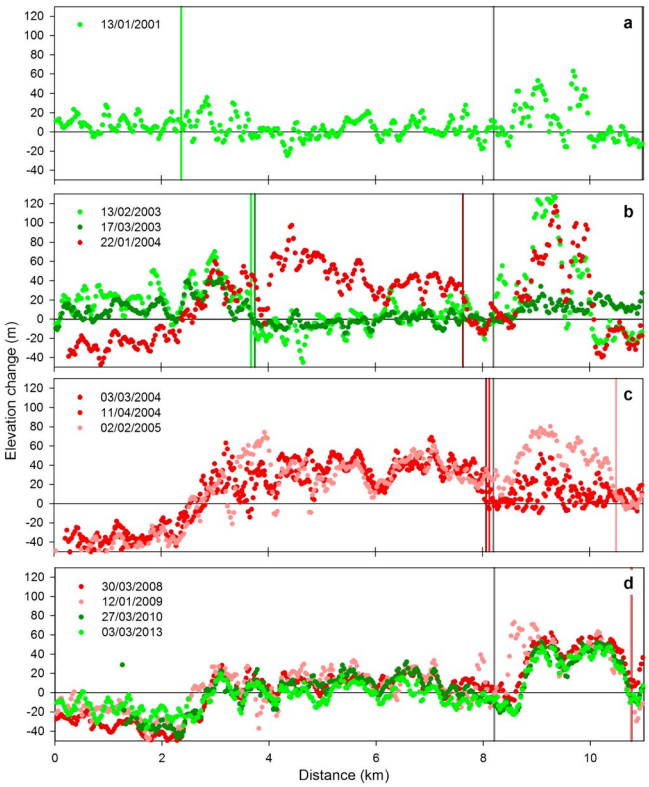

Figure 4. Elevation change profiles during the buildup (a), active (b-c) and depletion (d) phases of the HI surge. The active phase was separated in two (b and c) to depict the acceleration and slowdown. Elevation changes were calculated between each ASTER DEM (dates indicated in the legend) and the SRTM DEM (February 2000). Vertical lines show the position of the surge wave and the presurge position of the front (gray).

clearly a 2.7 km frontal advance that took place between 11 April 2004 and 2 February 2005 at a velocity of 9.1 m/d.

From 15 April 2005 to 25 November 2005 correlation failed again likely due to the reduction of moisture in the sediments at the glacier surface. This drying process is illustrated in Figure 5, where the glacier is increasingly harder to distinguish from the surrounding terrain. In this period the front advanced 0.29 km and further 0.01 km until 5 February 2006. The surface velocities of the lower reaches of the glacier decreased substantially in 2005 but were still around 0.3 m/d by 5 February 2006 (Figure 6). Afterward, the ice displacement becomes almost negligible, and therefore, we consider February 2006 as the termination date of the active phase.

The elevation profile steepened until 13 February 2003, when the reservoir zone (upper 3.7 km) thickened by 14 ± 16 m and the receiving zone was -2 ± 13 m below the 2001 level. The reservoir zone then lowered -72 ± 16 m until 2 February 2005 when it reached its minimum and later recovered 17 ± 13 m until the end of the active phase (5 February 2006). In contrast, the receiving zone experienced a -2 ± 9 m lowering until 13 February 2003 and then raised 36 ± 13 m when the surge wave overrode the lower portion of the glacier (11 April 2004).

The advance of the surge wave over the former glacier front position is evident in Figure 4c, where the elevation change of 2 February 2005 profile shows the occupation of the valley by a 48 ± 19 m thick glacier. This advance increased the length of the glacier from 8.2 to 10.5 km.

During the active phase a decoupling of the mean and the maximum velocities measured along the flow line was observed (Figure 6). Early in the active phase, the surge wave traveled toward the glacier front producing an initial peak of the mean and maximum velocities of the glacier. Then the velocities slowed-down markedly and the second peak showed a strong increase in the maximum velocity but only a moderate increase of the mean velocity. During this stage the surge wave overrode the front position and advanced rapidly, but the

Figure 5. Repeated field photos showing the evolution of the glacier surface during the surge. The location is "f" in Figure 1, facing north and is 11.5 km along the flow line. The 250 m wide valley was occupied by the advancing glacier; the presurge position was in the background, not captured in this frame. (a) Chaotic seracs and water-saturated sediment cover, during the advance of the glacier front. (b and c) Progressive meltdown and smoothing of the surface during the depletion phase. The water content of the sediment decreases and the glacier becomes less contrasted with the surrounding terrain.

rest of the glacier surface was already slowing down. This particular behavior indicates that the identification of a sudden glacier front advance is not necessarily a good record to assess the surge timing and magnitude.

3.3. Depletion Phase

After 5 February 2006 the ice velocities decreased to below 0.1 m/d, i.e., similar to presurge values, the velocity field did not show a coherent pattern and the terminus position of the glacier remained stable. Although some areas continued to exhibit localized motion (i.e., section 8.5–9.3 km, 0.3 m/d), most of the glacier surface was practically stagnant (Figure 3d).

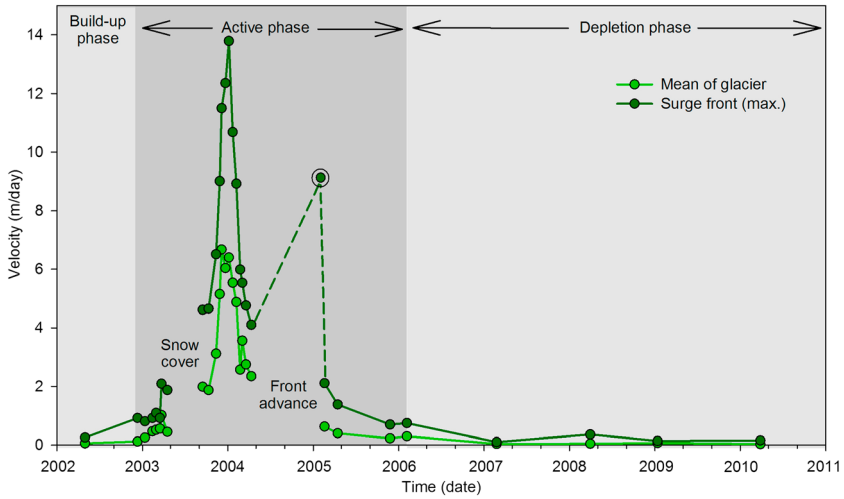

Figure 6. Mean and maximum velocities measured along the central flow line. The shading indicates the phase of the surge. Note that the image correlation failed during winter 2003 and again during the rapid advance of the glacier front (11 April 2004 to 2 February 2005). The dashed line and circled value indicate the measurement was calculated from the front advance instead of image correlation.

Between 24 February 2007 and 11 February 2014 the elevation of the reservoir zone increased by 16 ± 13 m, whereas the receiving zone lowered by 17 ± 4 m. The recovery of the reservoir zone and the lowering of the receiving zone resulted in a flattening of the postsurge elevation profile (Figure 4d).

3.4. Ice Volume Displacement

Around the peak of the surge, considered to have occurred between 17 March 2003 and 21 April 2004, the reservoir zone (upper 2.53 km^2) underwent an average elevation change of -43 ± 6 m and lost a total ice volume of 1.1 ± 0.2 10^8 m^3 (Figure 7a). The boundary between the reservoir and receiving zones, indicated

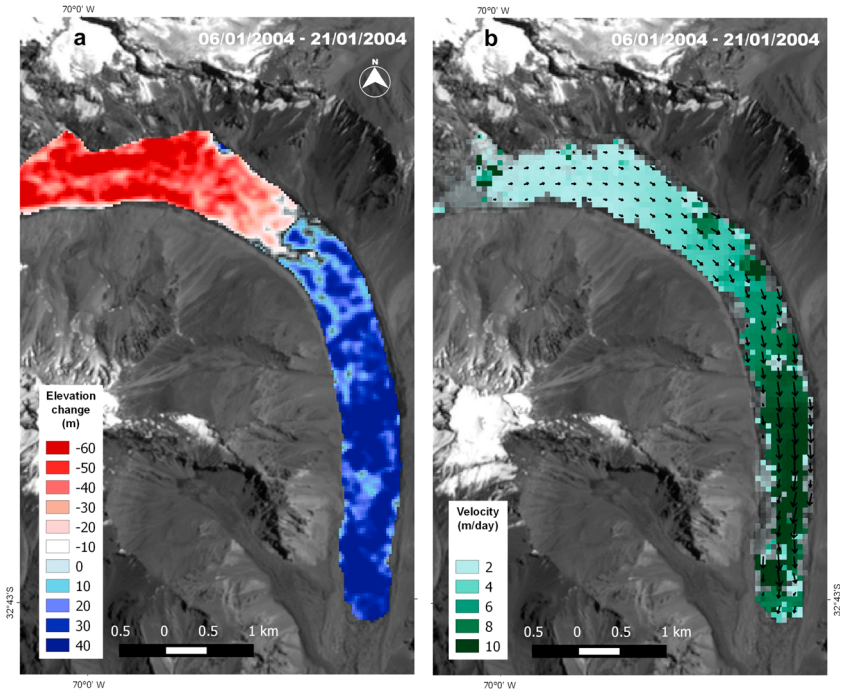

Figure 7. (a) Ice elevation changes between 17 March 2003 and 11 April 2004 derived from ASTER DEM. (b) Glacier velocity between 6 and 21 January 2004 derived from ASTER images.

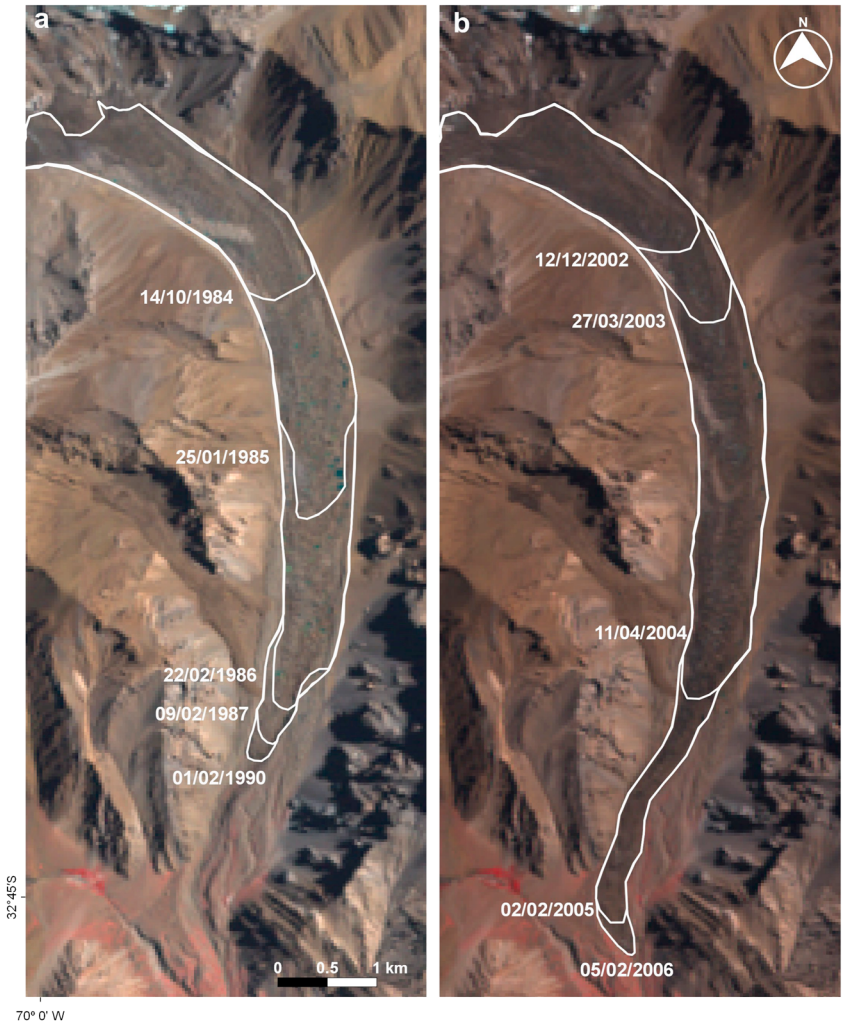

Figure 8. Evolution of two surge events in the Horcones Inferior Glacier: (a) 1984–1990 and (b) 2002–2006. The background images are 432 band composites of LANDSAT TM images of 1 February 1990 and 5 February 2006.

by an elevation change of 0 m, was identified at 4175 m asl, 3.4 km from the headwall, a location where the glacier is 0.7 km wide. The receiving zone covered 3.31 km^2 and thickened 30 ± 6 m, which resulted in a net gain of 1.0 ± 0.2 10^8 m^3 of ice in this period. Despite the relatively larger uncertainties involved, the volume change estimation of the receiving zone is likely more reliable than that in the upper zone. The quality of ASTER DEMs is better away from the steep south face of Mount Aconcagua, where seasonal snowfall can be observed in both scenes. Part of the 8% difference (corresponding to a mean rate of elevation change of −2.3 m/yr) between the volumes could also be due to ice melting during the almost 13 months separating the two DEMs. Melting of exposed ice, due to intense crevassing, can lead to high rates of back wasting, contributing disproportionately to glacier ablation [*Benn et al.*, 2012]. During this roughly 13 month period, an ice flux of about 10^8 m^3 was transferred through a 0.7 km wide gate at an average speed of 4.4 m/d suggesting a mean cross-section glacier thickness of ~90 m, which is in line with the 75–90 m reported in earlier studies [*Milana*, 2007].

3.5. Comparison With the 1984–1990 Event

The previous surge of HI has been studied through the examination of Landsat images and field surveys [*Happoldt and Schrott*, 1993; *Unger et al.*, 2000]. The earliest available image, 14 October 1984, indicates that the surge wave was at 5.83 km from the headwall and advanced 0.08 km at 0.8 m/d until 25 January 1985 (Figure 8a). A year later, on 22 February 1986, the surge front advanced another 2.78 km at a mean velocity

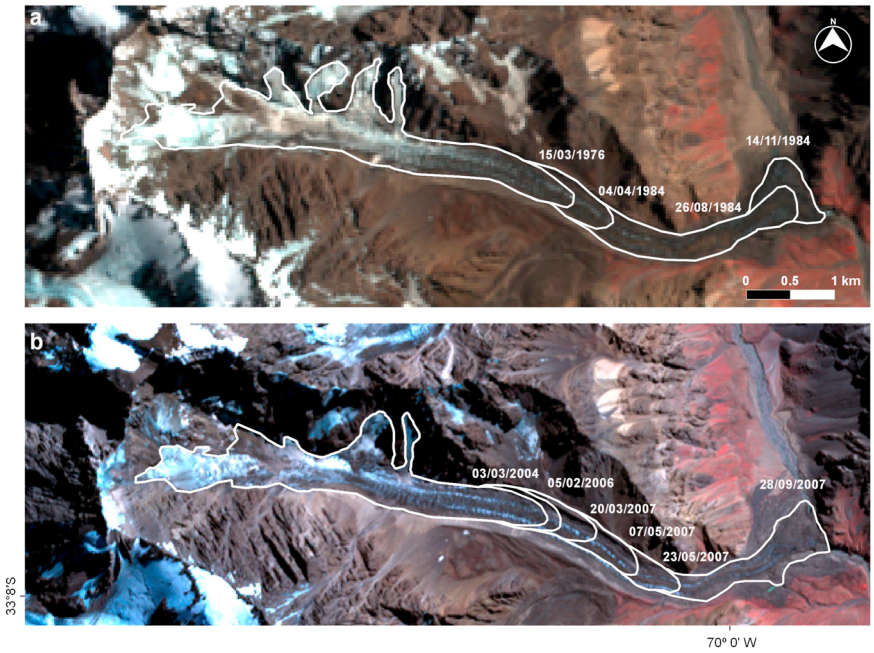

Figure 9. Surge wave evolution of the (a) 1984 and (b) 2004–2006 events of the Grande del Nevado Glacier. The background images are LANDSAT 432 band composites of 22 February 1986 and ASTER 321 band composite of 27 March 2010.

of 7.1 m/d. By 9 February 1987 the surge front had advanced an additional 0.41 km, at a mean velocity of 1.2 m/d. At some point before 22 February 1986 the surge wave overran the glacier front position and triggered an advance of 0.82 km until 1 February 1990. The surge front reached a height of 50 m in 1985 [*Happoldt and Schrott*, 1993].

The comparison between the two surges of HI is somewhat hampered by the sparser data on the 1984–1990 event. The velocities are similar at equivalent timescales: the mean velocity between 17 March 2003 and 19 March 2004 (384 days) was 6.52 m/d, while it was 7.07 m/d for 25 January 1985 to 22 February 1986 (397 days). The fastest velocities observed during the 2002–2006 event were measured at weekly to monthly resolutions, but such information is not available for the 1984–1990 event. The frontal advance was smaller (0.82 km) for the 1984–1990 event compared to 3.1 km for 2002–2006 (Figure 8). This result contrasts with other well-documented surging glaciers, with return times between 12 and 20 years, when more recent events have been observed to be less extensive (e.g., Lowell Glacier) [*Bevington and Copland*, 2014]. Finally, we found that the active phase of the 2002–2006 event lasted 3.1 years, while we estimated that the active phase of the 1984–1990 event lasted 5.3 years.

3.6. Surge of the Nearby Grande Del Nevado Glacier

The closest well-documented surging glacier in the region is the Grande del Nevado Glacier (see section 1), a 2.2 km^2, 4.7 km long, valley glacier with an elevation range of 1500 m (5200–3700 m asl). This glacier flows east on a tributary valley of the Plomo River. The Grande del Nevado Glacier has a history of three well-known surge events in 1933–1934 [*Helbling*, 1935], 1984–1985 [*Espizua and Bengochea*, 1990], and 2004–2007. Here we analyze the front position evolution of the two most recent events which coincide with the surges of HI. Between February and November 1984 the Grande del Nevado Glacier front advanced 2.5 km, with a maximum advance rate of 16 m/d between 4 April and 26 August 1984 (Figure 9). After 1985 the glacier apparently entered a quiescent phase until 2006 when a new advance was observed. Between 5 February 2006 and 26 September 2007 the glacier front advanced 3.0 km and reached a peak advance rate of 35 m/d between 7 and 23 May 2007. The comparison with the HI is somewhat hampered by the greater time steps between images in the Grande del Nevado Glacier, but there is a striking match in the active-phase timing. The Grande del Nevado Glacier appears to show faster velocities, which we consider to be related to differences in the morphology. Smaller area and length and greater elevation range and slope, all probably favor a faster propagation of the surge wave in the Grande del Nevado Glacier.

4. Discussion

4.1. Methodological Aspects

To our knowledge, we present the most complete time series of images used to study the geometric evolution of a glacier surge in the Andes. The coverage is particularly good for the active phase of the HI glacier surge, when 26 images are available. The mean interval between images is 59 days and is mainly determined by the lack of good images during the winter season. The summertime average interval is 23 days with several acquisitions only a week apart. This allowed us to correlate almost all available image pairs (except for the images of winter 2003), resulting in a very detailed data set of the surface velocity fields of the 2002–2006 surge event of HI.

Different factors can affect the performance of the image correlation. One case is the large motion of relatively narrow landforms such as HI. The sequential correlation implemented in COSI-Corr searches a larger area (initial window size) and once it succeeds, it searches a smaller area (final window size). If this procedure fails because the surface feature moved outside the window, an alternative to detect the large motion is to increase the initial correlation window size. A drawback of this solution is that the resulting motion fields can extend unrealistically into the surrounding stable terrain and introduce errors in the measurements. Another situation when correlation is compromised is the initial stage of the depletion phase when the motion is low but surface characteristics are changing. In other applications, such as earthquake analysis, fault line dominated by deformation separates large areas where the displacement is homogeneous and the correlation is well preserved [e.g., *Leprince et al*., 2007]. In glacier dynamics, the ice motion is accompanied with deformation so that with large displacements, surface features will deform, reducing the performance of the correlation. This is particularly evident in HI once the surge wave overrides the presurge glacier front, around 11 April 2004 (Figure 4), and the correlation failed due to the intense deformation. In those cases we manually measured the displacement of certain features, at the cost of losing the subpixel accuracy.

The 15 m spatial resolution of the ASTER images is close to the limit that can be used to monitor fast-flowing mountain glaciers of this size (~10 km^2). The use of 30 m spatial resolution Landsat images reduced the quality of the results. Higher-resolution images such as those provided by the Pléiades satellites can be correlated to resolve the small details of the glacier velocity field even on small to medium size glaciers [e.g., *Berthier et al*., 2014; *Ruiz et al*., 2015].

We believe the velocities measured during the active phase are likely reliable because (a) they are 1 to 2 orders of magnitude greater than the uncertainties (Figures 2a and 3) and (b) the velocity fields show high spatial consistency (Figure 7a). These results highlight the potential of the COSI-Corr routine to measure the motion of mountain glaciers with medium spatial resolution (15–30 m) satellite images acquired over short time intervals (weeks to months). In contrast, during the quiescent phase of the surge the uncertainties are in the same order of magnitude as the glacier velocities. In this case, the number of measurements is further reduced by the direction filter, reflecting the loss of the spatial consistency.

The elevation difference measurements have a larger uncertainty which can be, for individual pixels, in the same order of magnitude than the measurements (Figures 2b and 4). Nevertheless, the spatial patterns are consistent in the reservoir and receiving zones which increases our confidence on the signal (Figure 7b). Some features, typically tens-of-meters scale, are evident in the elevation profiles and appear to correspond to the major seracs that can be identified on the field. These are the "blocks" analyzed as an extensional fault system [*Milana*, 2007], which suggests that our elevation change maps can be used as an input for model approaches. The spatial resolution of the ASTER DEMs (30 m) is on the limit to individually track these features in time. In addition, the quality of the elevation data from ASTER DEM can be locally reduced due to artifacts and high-frequency noise [*Tachikawa et al*., 2011; *Frey and Paul*, 2012], as illustrated by the elevation change profiles in Figure 4. The poor quality of the data in front of the glacier tongue is likely due to the cast shading of the narrow valley walls. The elevation data improved once the glacier occupied the valley and became more continuous and less disperse (Figures 4c and 4d).

4.2. Glaciological Aspects

The acceleration of the ice during the surge was particularly strong and changed from an almost stagnant glacier into a fast flowing one in a period slightly longer than a year (Figure 5). The short-lived active phase and decade long quiescent phase make glaciers in the Andes more akin to those observed in the Karakoram

[*Quincey et al*., 2011] and Pamir [*Kotlyakov et al*., 2008], rather than to the decadal-long active phase and sometimes over a century-long quiescent phase observed in higher-latitude locations such as Greenland and Svalbard [*Jiskoot et al*., 1998].

The large advance (3.1 km) observed in the HI front position is at odds with the behavior of other glaciers in the region which have shown a moderate recession in the same period [*Espizua and Pitte*, 2009]. Between 2004 and 2005 the surge wave advanced on bare ground (glacier front advance), and the image cross correlations failed. Unfortunately, this period also coincided with an interval of 297 days without images. We measured an average velocity for the glacier front advance of 9.1 m/d, which is much lower than the 28 m/d reported from field observation during the summer of 2004–2005 [*Francou and Vincent*, 2007]. This discrepancy is thought to be largely due to the different time steps in the measurements between images (weeks to months) and the daily field survey. After 5 February 2006, the velocities over most of the glacier decreased and no more significant motion was observed. This was confirmed by Global Navigation Satellite Systems measurements during 2009–2010 that yielded velocities lower than 0.03 m/d [*Lenzano et al*., 2013].

Due to the number of satellite images (32) compiled in this study, the duration of the active phase is well constrained: 3.16 years, i.e., lasting from December 2002 to February 2006. The duration was found to be longer than suggested in previous reports, which indicated the surge occurred between February 2003 and January 2006 [*Espizua et al*., 2008], January 2004 and July 2005 [*Francou and Vincent*, 2007], and October 2003 and February 2006 [*Lenzano et al*., 2011]. Regularly acquired satellite images are probably the best way to establish an accurate timing of the surging events, which in turn is a key to explore the connections between climate and the recurrence intervals of the surging events. This is well illustrated with the findings on HI, where the full extent of the surge was inaccurately known until this study, despite being one of the most accessible and visited glacier of the Central Andes.

The relation between the surge of glaciers and avalanches or rockslides has been controversial in this part of the Andes. In the initial report describing the 1930s event of the Grande del Nevado Glacier, the whole ice mass (4.5 km long, 0.2 to 0.6 km wide, 80 m thick, and 5.4 10^7 m^3) obstructing the Plomo River was described as an avalanche [*King*, 1934]. Responding to this report, *Helbling* [1935] argued that the geomorphological evidence such as the stratification of the ice, the transversal crevassing, the lake formation in different stages, and the existence of previous moraines, all indicated that the glacier had advanced. The author estimated that it would take an unrealistic 30 m snowfall over the feeding area to produce an avalanche with the observed volume, but did concede that avalanching in the upper reaches could be one of triggers of the glacier advance. Similar arguments were also introduced in the HI. The deposits described as Horcones moraine have been reinterpreted as deposits from a large postglacial rockslide [*Fauqué et al*., 2009]. These authors argue that a part of the current hanging glaciers of the south face of Mount Aconcagua collapsed 10000–13000 years ago and produced a 20 km saturated flow overriding the existing glacier, in similar way to the tragic events of the Nevado Huascarán, Perú, in 1970 [*Plafker*, 1971]. For the most recent event of HI (2002–2006) a large avalanche from the hanging glaciers of the Aconcagua south face has also been mentioned as a possible trigger [*Lenzano et al*., 2011]. The findings in our work indicate that the glacier advances are due to dynamic instability spanning several years rather than to a single catastrophic event. In return, avalanching from hanging glaciers contributes to both the HI and the Grande del Nevado glaciers. This process could be increased by positive mass balance, but no information on avalanches frequency and intensity is available.

The large volume of ice displaced during the surge (10^8 m^3) is currently experiencing rapid melting and down wasting (Figure 4d). The relatively high rates of surface lowering in the receiving zone will further flatten the surface profile. In turn, this results in reduced driving stresses encouraging glacier slowdown and stagnation [*Benn et al*., 2012]. Additionally, this is a source of meltwater, especially considering the unprecedented multiyear drought that is affecting this semiarid region since 2010. Over the past 5 years the Mendoza River (the river supporting the largest population in central-western Argentina) has drained only ~10^9 m^3 of water annually.

4.3. Climatic Influence on Surge Recurrence Interval

The cumulative mass balance has been proposed as a modulator of the surge recurrence interval in different studies [*Meier and Post*, 1969; *Eisen et al*., 2001; *Harrison and Post*, 2003; *Tangborn*, 2013]. Here we interpret the synchronicity of the best studied surges in the region, HI and Grande del Nevado glaciers, to be an indicator of such modulation. Further research on other surging glaciers is required to adequately investigate and

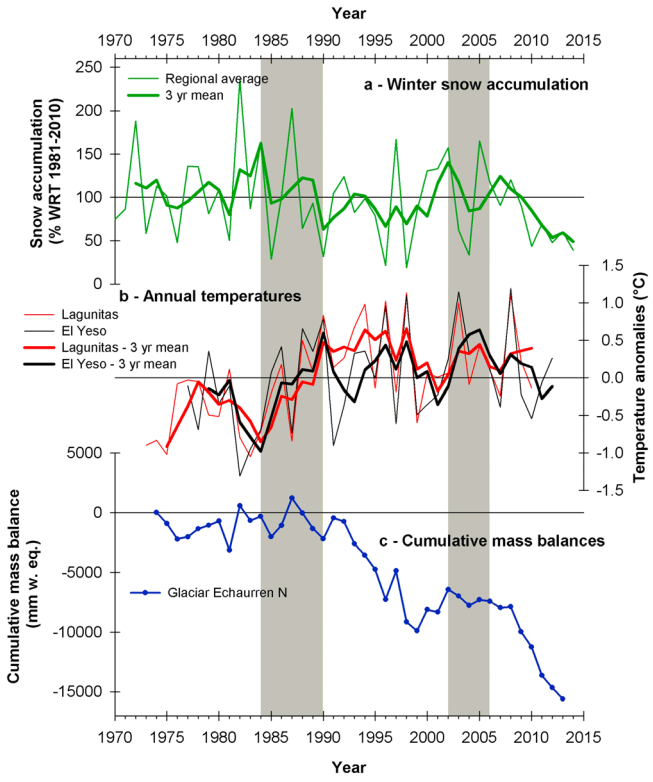

Figure 10. Snow accumulation, temperature, and mass balance in the Central Andes. (a) Regional average of snow accumulation (percentage with respect to the 1981–2010 period) with 3 year running mean. (b) Annual temperature anomalies at El Yeso (33.68°S, 70.09°W, 2475 m asl) and Lagunitas (33.08°S, 70.25°W, 2765 m asl) stations with 3 year running mean. (c) Cumulative mass balance of Echaurren Norte Glacier (1973–2013). Shading indicates the active phase of the recent surges of Horcones Inferior and Grande del Nevado Glaciers.

support this relation. We expect that ongoing work, partly based on DEM differencing and refined with ASTER velocity mapping, will greatly expand the number of surge-type glaciers and events documented for the Central Andes.

In the 9 years prior to the surge events the available data show mostly above-average snow accumulation [*Masiokas et al.*, 2006, 2010] and below-average temperatures (Figures 10a and 10b). The wettest period in the region was 1977–1987 and encompassed the buildup and most of the active phase of surge events of the HI and Grande del Nevado glaciers. Afterward, generally dry conditions were observed until 1999 when another relatively wet interval persisted until 2009. The buildup and active phase of the most recent surge in both HI and Grande del Nevado glaciers also coincided with this period. In this arid region, the dominance of winter accumulation on the annual mass balance is well known [*Rabatel et al.*, 2011]. The mass balance of the small Echaurren Norte Glacier (95 km to the south east of HI) [*Escobar et al.*, 1995; *WGMS*, 2013] shows two intervals of positive balance embedded in a long-term negative trend of cumulative mass balance (1979 to 2013, −15 m w.e, Figure 10c). Temperatures from the nearest station with long, complete data (El Yeso, 33.68°S, 70.09°W, 2475 m asl and Lagunitas 33.08°S, 70.25°W, 2765 m asl) show below-average temperatures before the events (1984–1990 and 2003–2007), followed by a rise at the onset of the active phase. Here we hypothesize that large accumulation and low temperatures contributed to positive mass balances during the buildup phase and may have contributed to the initiation of the active phase of the surge of these two glaciers.

4.4. Comparison With Karakoram Glacier Surges

Several characteristics of the surge-type glaciers identified in the Central Andes are found in the Karakoram. This heavily glacierized mountain range, about 500 km long, contains several of the world's highest peaks and is located mostly in Pakistan, India, and China. The semiarid and strongly continental climate with strong winds, great diurnal ranges of temperature, and intensive solar radiation favors the development of "penitentes" and debris-covered glaciers [*Hewitt*, 1969]. All these factors make the Karakoram a good analogue to the Central Andes, as already noted by *Helbling* [1935]. In the Karakoram 101 documented surges-type glaciers were identified [*Rankl et al.*, 2014], which represents about 13% of all glaciers in the region [*Barrand and Murray*, 2006].

Observed velocities in the Karakoram are below 5 m/d for periods that typically range between 1 and 2 months [*Mayer et al.*, 2011; *Rankl et al.*, 2014; *Quincey et al.*, 2015]. This is lower than the velocities reported in our work. We attribute this difference partly to the fact that our time series is exceptionally dense and captures the maximum velocities on a week-to-month scale. Elevation changes in the reservoir and receiving zones are reported to be up to 16 m/yr [*Gardelle et al.*, 2013], comparable to the changes described for HI.

In the Karakoram surging glaciers were found to be correlated to glacier length (larger than 4 km), area, perimeter, and debris cover [*Barrand and Murray*, 2006], all of which apply to known surging glaciers in the Central Andes. Perimeter was suggested to be related to the avalanching processes feeding many of these glaciers which also holds true for HI and Grande del Nevado. In addition, the recurrence interval of the events identified in the Karakoram is ~20–45 years [*Copland et al*., 2011; *Quincey and Luckman*, 2014], which is consistent with the timing of the two most recent events of HI and Grande del Nevado glaciers.

5. Conclusions

This study provides a comprehensive coverage of the most recent (2002–2006) surge event of the Horcones Inferior Glacier in the Central Andes of Argentina (~32°S), based on the calculation of velocity fields and elevation change maps. The maximum velocities (14 m/d), the advance of the front (3.1 km), and the phase durations are similar to those reported for surges in other regions (Karakoram, Alaska). The spatial and temporal coverage obtained for the HI is unprecedented for the study region.

The uncertainties of the displacements, estimated on stable control areas, are subpixel (one fifth for ASTER and one fourth to one half for Landsat ETM+ and TM) and at least an order of magnitude lower than the measured peak velocities. This adds to existing work showing that image cross correlation as implemented in COSI-Corr is an efficient and powerful tool for measuring glacier displacements with multitemporal medium spatial resolution (15–30 m) images. We also obtained the first estimate of the volume of ice (about 10^8 m^3) transferred during the peak of the HI surge. Combining the elevation change measurements with the velocity data, we derived a first order estimate of ~90 m for the mean glacier thickness through the cross section separating the reservoir from the receiving zones.

The initiation of the active phase in spring, the abrupt change between quiescent and active-phase velocities, the relatively short duration of the surge cycle, and the abnormally high stream flow levels all point to a hydrological switch (Alaskan type) mechanism. Reliable information from HI and Grande del Nevado glaciers, although limited, indicates an influence of climate, through a cumulative positive anomaly in accumulation, on the recurrence interval of the surge events. An analogy with the much better studied Karakoram glaciers where 13% of glaciers are known to be surge type suggests that a large number of surges in the Central Andes could still be unreported. Future studies will include the Plomo massif where other glaciers, besides Grande del Nevado, are also thought to be surge type [*Helbling*, 1935].

Acknowledgments

The data for this paper are available by contacting the corresponding author. The ASTER images and DEM used in this paper were available through the GLIMS project [*Kargel et al*., 2014], for which IANIGLA-CONICET is a regional center. We would like to thank Bruce Raup, Jeff Kargel, and Silvia Delgado who fostered this collaboration. Images and DEMs were downloaded from the USGS Global Visualization Viewer (http://glovis.usgs.gov/) which is one of the Earth Resources Observation and Science Center sites. We thank Fabián Díaz and Pablo Lizana for field data and photos and the Parque Provincial Aconcagua for granting access to the HI. We are grateful to the Editor, the Associate Editor, and the three anonymous reviewers who provided many insightful comments to improve this manuscript. Etienne Berthier is supported by the French Space Agency (CNES) through the TOSCA program.

References

Barrand, N. E., and T. Murray (2006), Multivariate controls on the incidence of glacier surging in the Karakoram Himalaya, *Arct. Antarct. Alp. Res.*, *38*(4), 489–498.

Benn, D. I., T. Bolch, K. Hands, J. Gulley, A. Luckman, L. I. Nicholson, D. Quincey, S. Thompson, R. Toumi, and S. Wiseman (2012), Response of debris-covered glaciers in the Mount Everest region to recent warming, and implications for outburst flood hazards, *Earth Sci. Rev.*, *114*(1–2), 156–174, doi:10.1016/j.earscirev.2012.03.008.

Berthier, E., and T. Toutin (2008), SPOT5-HRS digital elevation models and the monitoring of glacier elevation changes in North-West Canada and South-East Alaska, *Remote Sens. Environ.*, *112*(5), 2443–2454.

Berthier, E., H. Vadon, D. Baratoux, Y. Arnaud, C. Vincent, K. L. Feigl, F. Rémy, and B. Legrésy (2005), Surface motion of mountain glaciers derived from satellite optical imagery, *Remote Sens. Environ.*, *95*(1), 14–28, doi:10.1016/j.rse.2004.11.005.

Berthier, E., E. Schiefer, G. K. C. Clarke, B. Menounos, and F. Rémy (2010), Contribution of Alaskan glaciers to sea-level rise derived from satellite imagery, *Nat. Geosci.*, *3*, 92–95.

Berthier, E., et al. (2014), Glacier topography and elevation changes derived from Pléiades sub-meter stereo images, *Cryosphere*, *8*, 2275–2291, doi:10.5194/tc-8-2275-2014.

Bevington, A., and L. Copland (2014), Characteristics of the last five surges of Lowell Glacier, Yukon, Canada, since 1948, *J. Glaciol.*, *60*(219), 113–123.

Björnsson, H., F. Pálsson, O. Sigurḥsson, and G. E. Flowers (2003), Surges of glaciers in Iceland, *Ann. Glaciol.*, *36*(1), 82–90.

Carrasco, J., R. Osorio, and G. Cassasa (2008), Secular trend of the ELA on the western side of the southern Andes, derived from radiosonde and surface observations, *J. Glaciol.*, *54*, 538–550.

Copland, L., T. Sylvestre, M. P. Bishop, J. F. Shroder, Y. B. Seong, L. A. Owen, A. Bush, and U. Kamp (2011), Expanded and recently increased glacier surging in the Karakoram, *Arct. Antarct. Alp. Res.*, *43*(4), 503–516, doi:10.1657/1938-4246-43.4.503.

Cuffey, K. M., and W. S. B. Paterson (2010), *The Physics of Glaciers*, *Glaciology*, 4th ed., Butterworth-Heinemann/Elsevier, Burlington, Mass.

Dolgoushin, L. D., and G. B. Osipova (1975), Glacier surges and the problem of their forecasting, *IAHS-AISH Publ.*, *104*, 292–304.

Eisen, O., W. D. Harrison, and C. F. Raymond (2001), The surges of Variegated Glacier, Alaska, USA, and their connection to climate and mass balance, *J. Glaciol.*, *47*(158), 351–358.

Escobar, F., G. Casassa, and V. Pozo (1995), Variaciones de un glaciar de montaña en los Andes de Chile Central en las últimas dos décadas, *Bull. de l'Inst. Français d'Études Andines*, *24*, 683–695.

Espizua, L., and P. Pitte (2009), The Little Ice Age advance in the Central Andes (35°S) Argentina, *Palaeogeogr. Palaeoclimatol. Palaeoecol.*, *281*, 345–350.

Espizua, L. E., and J. D. Bengochea (1990), Surge of Grande del Nevado Glacier (Mendoza, Argentina) in 1984: Its evolution through satellite images, *Geogr. Ann. Ser. A, Phys. Geogr.*, *72*(3/4), 255, doi:10.2307/521153.
Espizua, L. E., P. Pitte, and L. Ferri Hidalgo (2008), Horcones Inferior Glacier surge, in *Fluctuations of Glaciers, 2000–2005*, vol. 9, pp. 43–44, WGMS, Zurich, Switzerland.
Farr, T. G., et al. (2007), The Shuttle Radar Topography Mission, *Rev. Geophys.*, *45*, RG2004, doi:10.1029/2005RG000183.
Fauqué, L., R. Hermanns, K. Hewitt, M. Rosas, C. Wilson, V. Baumann, S. Lagorio, and I. Di Tommaso (2009), Mega-deslizamientos de la pared sur del Cerro Aconcagua y su relación con depósitos asignados a la glaciación Pleistocena, *Rev. Asoc. Geol. Argent.*, *65*(4), 691–712.
Francou, B., and C. Vincent (2007), *Les glaciers a l'epreuve du climat*, *Glaciology*, IRD Editions, Belin, Paris, France.
Frey, H., and F. Paul (2012), On the suitability of the SRTM DEM and ASTER GDEM for the compilation of topographic parameters in glacier inventories, *Int. J. Appl. Earth Obs. Geoinf.*, *18*, 480–490, doi:10.1016/j.jag.2011.09.020.
Gardelle, J., E. Berthier, Y. Arnaud, and A. Kääb (2013), Region-wide glacier mass balances over the Pamir-Karakoram-Himalaya during 1999–2011, *Cryosphere*, *7*(4), 1263–1286, doi:10.5194/tc-7-1263-2013.
Happoldt, H., and L. Schrott (1993), Horcones Inferior—Glacier surge, in *Fluctuations of Glaciers 1985–1990*, vol. 6, pp. 70, IAHS (ICSI)/UNEP/UNESCO, Zurich, Switzerland.
Harrison, W. D., and A. S. Post (2003), How much do we really know about glacier surging?, *Ann. Glaciol.*, *36*(1), 1–6.
Helbling, R. (1935), The origin of the Rio Plomo ice-dam, *Geogr. J.*, *85*(1), 41, doi:10.2307/1787035.
Herman, F., B. Anderson, and S. Leprince (2011), Mountain glacier velocity variation during a retreat/advance cycle quantified using sub-pixel analysis of ASTER images, *J. Glaciol.*, *57*(202), 197–207.
Hewitt, K. (1969), Glacier surges in the Karakoram Himalaya (Central Asia), *Can. J. Earth Sci.*, *6*(4), 1009–1018.
Hirano, A., R. Welch, and H. Lang (2003), Mapping from ASTER stereo image data: DEM validation and accuracy assessment, *J. Photogramm. Remote Sens.*, *57*, 356–370.
Jiskoot, H., and D. T. Juhlin (2009), Surge of a small East Greenland glacier, 2001–2007, suggests Svalbard-type surge mechanism, *J. Glaciol.*, *55*(191), 567–570.
Jiskoot, H., P. Boyle, and T. Murray (1998), The incidence of glacier surging in Svalbard: Evidence from multivariate statistics, *C. R. Geosci.*, *24*(4), 387–399.
Jiskoot, H., T. Murray, and A. Luckman (2003), Surge potential and drainage-basin characteristics in East Greenland, *Ann. Glaciol.*, *36*(1), 142–148.
Kamb, B. (1987), Glacier surge mechanism based on linked cavity configuration of the basal water conduit system, *J. Geophys. Res.*, *92*(B9), 9083–9100, doi:10.1029/JB092iB09p09083.
Kargel, J. S., G. J. Leonard, M. P. Bishop, A. Kääb, and B. H. Raup (Eds) (2014), *Global Land Ice Measurements from Space*, *Ice Snow Remote Sens.- Glaciol.*, Springer, Berlin, Heidelberg.
King, W. D. V. O. (1934), The Mendoza River flood of 10–11 January 1934—Argentina, *Geogr. J.*, *84*(4), 321, doi:10.2307/1786696.
Kotlyakov, V. M., G. B. Osipova, and D. G. Tsvetkov (2008), Monitoring surging glaciers of the Pamirs, central Asia, from space, *Ann. Glaciol.*, *48*(1), 125–134.
Leiva, J. C., G. A. Cabrera, and L. E. Lenzano (2007), 20 years of mass balances on the Piloto glacier Las Cuevas river basin, Mendoza, Argentina, *Global Planet. Change*, *59*, 10–16.
Lenzano, M. G., J. C. Leiva, D. Trombotto, and L. Lenzano (2011), Satellite images and geodetic measurements applied to the monitoring of the Horcones Inferior Glacier, Mendoza, Argentina, *Geoacta*, *36*, 13–25.
Lenzano, M. G., L. Lenzano, D. T. Liaudat, J. Barón, and E. Lannutti (2013), Applying GNSS and DTM technologies to monitor the ice balance of the Horcones Inferior Glacier, Aconcagua Region, Argentina, *J. Indian Soc. Remote Sens.*, *41*(4), 969–980, doi:10.1007/s12524-013-0294-z.
Leprince, S., S. Barbot, F. Ayoub, and J.-P. Avouac (2007), Automatic and Precise Orthorectification, Coregistration, and Subpixel Correlation of Satellite Images, Application to Ground Deformation Measurements, *IEEE Trans. Geosci. Remote Sens.*, *45*(6), 1529–1558, doi:10.1109/TGRS.2006.888937.
Lliboutry, L. (1956), *Nieve y Glaciares de Chile. Fundamentos de Glaciología*, *Glaciology*, Ediciones de la Universidad de Chile, Santiago, Chile.
Lliboutry, L. (1999), Glaciers of Chile and Argentina, in *Satellite Image Atlas of Glaciers of the World. South America*, vol. 1386-I, edited by R. S. Williams and J. G. Ferrigno, USGS, Denver, Colo.
Masiokas, M., R. Villalba, B. Luckman, C. Le Quesne, and J. C. Aravena (2006), Snowpack variations in the Central Andes of Argentina an Chile, 1951–2005: Large-scale atmospheric influences and implications for water resources in the region, *J. Clim.*, *19*, 6334–6352.
Masiokas, M., R. Villalba, B. Luckman, and S. Mauget (2010), Intra- to multi-decadal variations of snowpack and streamflow records in the Andes of Chile and Argentina between 30° and 37°S, *J. Hydrometeorol.*, *2*, 822–831.
Masiokas, M. H., A. Rivera, L. E. Espizua, R. Villalba, S. Delgado, and J. C. Aravena (2009), Glacier fluctuations in extratropical South America during the past 1000 years, *Palaeogeogr. Palaeoclimatol. Palaeoecol.*, *281*, 242–268.
Mayer, C., A. C. Fowler, A. Lambrecht, and K. Scharrer (2011), A surge of North Gasherbrum Glacier, Karakoram, China, *J. Glaciol.*, *57*(205), 904–916.
Meier, M. F., and A. Post (1969), What are glacier surges?, *Can. J. Earth Sci.*, *6*(4), 807–817.
Milana, J. P. (2007), A model of the Glaciar Horcones Inferior surge, Aconcagua region, Argentina, *J. Glaciol.*, *53*(183), 565–572.
Murray, T., T. Strozzi, A. Luckman, H. Jiskoot, and P. Christakos (2003), Is there a single surge mechanism? Contrasts in dynamics between glacier surges in Svalbard and other regions, *J. Geophys. Res.*, *108*(B5), 2273, doi:10.1029/2002JB001906.
Paul, F., et al. (2013), On the accuracy of glacier outlines derived from remote-sensing data, *Ann. Glaciol.*, *54*, 171–182, doi:10.3189/2013AoG63A296.
Plafker, G. (1971), Geological aspects of the May 31, 1970 Perú earthquake, *Bull. Seismol. Soc. Am.*, *61*(3), 543–578.
Post, A. (1969), Distribution of surging glaciers in western North America, *J. Glaciol.*, *8*(53), 229–240.
Quincey, D. J., and A. Luckman (2014), Brief communication: On the magnitude and frequency of Khurdopin glacier surge events, *Cryosphere*, *8*(2), 571–574, doi:10.5194/tc-8-571-2014.
Quincey, D. J., M. Braun, N. F. Glasser, M. P. Bishop, K. Hewitt, and A. Luckman (2011), Karakoram glacier surge dynamics, *Geophys. Res. Lett.*, *38*, L18504, doi:10.1029/2011GL049004.
Quincey, D. J., N. F. Glasser, S. J. Cook, and A. Luckman (2015), Heterogeneity in Karakoram glacier surges, *J. Geophys. Res. Earth Surf.*, *120*, 1288–1300, doi:10.1002/2015JF003515.
Rabatel, A., H. Castelbrunet, V. Favier, L. Nicholson, and C. Kinnard (2011), Glacier changes in the Pascua-Lama region, Chilean Andes (29°S): Recent mass-balance and 50 year surface-area variation, *Cryosphere*, *5*, 1029–1041.
Rankl, M., C. Kienholz, and M. Braun (2014), Glacier changes in the Karakoram region mapped by multimission satellite imagery, *Cryosphere*, *8*(3), 977–989, doi:10.5194/tc-8-977-2014.

Rothlisberger, F. (1986), 10.000 Jahre Gletschergeshichte de Erde: ein Vergleich zwischen Nord und Sudhemisphäre Glacier fluctuations, Sauerlander.

Ruiz, L., E. Berthier, M. Masiokas, P. Pitte, and R. Villalba (2015), First surface velocity maps for glaciers of Monte Tronador, North Patagonian Andes, derived from sequential Pleiades satellite images, *J. Glaciol.*, *61*(229), 1–15, doi:10.3189/2015JoG14J134.

Scherler, D., S. Leprince, and M. Strecker (2008), Glacier-surface velocities in alpine terrain from optical satellite imagery—Accuracy improvement and quality assessment, *Remote Sens. Environ.*, *112*(10), 3806–3819, doi:10.1016/j.rse.2008.05.018.

Sevestre, H., and D. I. Benn (2015), Climatic and geometric controls on the global distribution of surge-type glaciers: Implications for a unifying model of surging, *J. Glaciol.*, *61*(228), doi:10.3189/2015JoG14J136.

Tachikawa, T., et al. (2011), ASTER Global Digital Elevation Model Version 2—Summary of validation results ASTER GDEM 2, NASA-LPDACC.

Tangborn, W. (2013), Mass balance, runoff and surges of Bering Glacier, Alaska, *Cryosphere*, *7*(3), 867–875, doi:10.5194/tc-7-867-2013.

Truffer, M., W. D. Harrison, and K. A. Echelmeyer (2000), Glacier motion dominated by processes deep in underlying till, *J. Glaciol.*, *46*(153), 213–221.

Unger, C., L. E. Espizua, and R. Bottero (2000), Untersuchung von gletscherständen im Tal des Rio Mendoza (zentralargentinische Anden) - kartierung eines surge-vorstosses des Horcones Inferior, *Z. Gletsch.kd. Glazialgeol.*, *36*, 151–157.

World Glacier Monitoring Service (WGMS) (2013), *Glacier mass balance bulletin. Bulletin No. 12 (2010–2011), Mass Balance—World*, UNESCO, Zurich, Switzerland.